



Contents lists available at ScienceDirect

Journal of Biomechanics

journal homepage: www.elsevier.com/locate/jbiomech
www.JBiomech.com

Wide-range dynamic magnetic resonance elastography

Kerstin Riek^a, Dieter Klatt^b, Hassan Nuzha^b, Susanne Mueller^c, Ulf Neumann^d,
Ingolf Sack^b, Jürgen Braun^{a,*}

^a Department of Medical Informatics, Charité—Universitätsmedizin Berlin, Campus Benjamin Franklin, Hindenburgdamm 30, 12203 Berlin, Germany

^b Department of Radiology, Charité—Universitätsmedizin Berlin, Campus Charité Mitte, Berlin, Germany

^c Center for Stroke Research Berlin—Universitätsmedizin Berlin, Campus Charité Mitte, Berlin, Germany

^d Department of General, Visceral, and Transplant Surgery, Charité—Universitätsmedizin Berlin, Campus Virchow-Klinikum, Berlin, Germany

ARTICLE INFO

Article history:

Accepted 25 December 2010

Keywords:

Complex modulus dispersion
Shear oscillation
Imaging
Fractional element
Liver fibrosis
Brain
Muscle
Wave scattering

ABSTRACT

Tissue mechanical parameters have been shown to be highly sensitive to disease by elastography. Magnetic resonance elastography (MRE) in the human body relies on the low-dynamic range of tissue mechanics < 100 Hz. In contrast, MRE suited for investigations of mice or small tissue samples requires vibration frequencies 10–20 times higher than those used in human MRE. The dispersion of the complex shear modulus (G^*) prevents direct comparison of elastography data at different frequency bands and, consequently, frequency-independent viscoelastic models that fit to G^* over a wide dynamic range have to be employed. This study presents data of G^* of samples of agarose gel, liver, brain, and muscle measured by high-resolution MRE in a 7T-animal scanner at 200–800 Hz vibration frequency. Material constants μ and α according to the springpot model and related to shear elasticity and slope of the G^* -dispersion were determined. Both μ and α of calf brain and bovine liver were found to be similar, while a sample of fibrotic human liver (METAVIR score of 3) displayed about fifteen times higher shear elasticity, similar to μ of bovine muscle measured in muscle fiber direction. α was the highest in fibrotic liver, followed by normal brain and liver, while muscle had the lowest α -values of all biological samples investigated in this study. As expected, the least G^* -dispersion was seen in soft gel. The proposed technique of wide-range dynamic MRE can provide baseline data for both human MRE and high-dynamic MRE for better understanding tissue mechanics of different tissue structures.

© 2011 Elsevier Ltd. All rights reserved.

1. Introduction

Shear viscoelastic properties are sensitive to the microstructural constitution and physiological state of biological tissues. Changes in the mechanical properties of living tissue can indicate disease progression as in liver fibrosis (Ziol et al., 2005; Yin et al., 2007; Huwart et al., 2007), physiological processes such as normal aging of cerebral tissue (Sack et al., 2009), or the establishment of myosin cross-links with muscle contraction (Hoyt et al., 2008; Gennisson et al., 2010). Researchers today use elastography to gain insights into the relationship between disease and tissue mechanics. Elastography combines mechanical stimulation of tissue by shear waves or by static compression with medical ultrasound or magnetic resonance imaging (Ophir et al., 1991; Muthupillai et al., 1995). Shear-wave-based ultrasound elastography has been used to measure viscoelasticity of skeletal muscle and liver by means of the dispersion of the wave propagation speed within a frequency range 80–800 Hz (Hoyt et al., 2008; Deffieux et al., 2009; Gennisson et al., 2010). In contrast,

multifrequency magnetic resonance elastography (MRE) relies on the inversion of complex shear wave images after Fourier decomposition of time-harmonic vibrations (Klatt et al., 2007). This strategy directly yields the dispersion of the complex shear modulus, G^* , which has been analyzed in liver (Asbach et al., 2008, 2010), brain (Sack et al., 2009; Wuerfel et al., 2010), and skeletal muscle (Klatt et al., 2010b) in a frequency range between 25 and 62.5 Hz. The dynamic range of MRE can be extended by invasive tests (Vappou et al., 2007) or in vivo mouse MRE, where the range of frequencies is between 200 and 1200 Hz due to a smaller field of view and higher gradient strengths (Othman et al., 2005; Atay et al., 2008; Salameh et al., 2009). However, few elastography data have been reported on the dynamics of the complex shear modulus in this frequency range, and their comparison to the low-dynamic range applicable to humans is still vague. This “missing link” between high-dynamic MRE and human MRE might be resolved by applying identical models of the viscoelastic behavior of tissue in order to deduce comparable (frequency-independent) material constants. Therefore this study aims to investigate the complex modulus dispersion of tissue samples in a 7T animal MRI scanner over a wide dynamic range. Three types of biological tissue are investigated: bovine skeletal muscle, bovine liver, and calf brain.

* Corresponding author. Tel.: +49 30 450 539098; fax: +49 30 450 544901.
E-mail address: juergen.braun@charite.de (J. Braun).

Additionally, a sample of human fibrotic liver is tested to identify any changes in G^* dispersion due to disease. The variation in G^* dynamics is analyzed and discussed in terms of two viscoelastic variables, μ and α , according to the so-called springpot model. It serves as basic element in fractional generalizations of standard linear viscoelastic models (Schuessel and Blumen, 1995). Linear viscoelastic models can be extended to their fractional generalization by replacing the basic rheological elements “spring” and “dashpot” with the springpot. In contrast to the Voigt model which comprises a constant storage modulus, the springpot is an inherent powerlaw model. Thus it allows reproducing a monotonic increase in both storage modulus (real part of G^*) and loss modulus (imaginary part of G^*) over frequency by only two variables. While μ relates to the inherent connectivity and adhesion of the mechanical matrix of tissue, α is associated with the micro-geometry and alignment of tissue building blocks. These parameters have been used to analyze the powerlaw in G^* observed by in vivo MRE in various human organs (Sinkus et al., 2007; Sack et al., 2009; Asbach et al., 2010; Klatt et al., 2010b). According to the model of generalized Gaussian structures (Gurtovenko and Blumen, 2005) the α -parameter, i.e. the power of the G^* -dispersion in the so-called intermediated dynamic range, is related to the degree of freedoms of the underlying mechanical network (Klatt et al., 2010b). We can thus learn from high-dynamic MRE how viscoelastic properties of biological tissue relate to structure and disease, which can provide the background for in-depth analysis of in vivo human MRE data.

2. Materials and methods

2.1. Sample material and preparation

Fresh bovine liver, bovine muscle, and calf brain were obtained from a slaughterhouse a few hours before the experiments. A sample of human fibrotic liver (biopsy-proven METAVIR score 3) was obtained from the Department of Transplant Surgery of the Charité—Universitätsmedizin Berlin and examined by MRE within 2 h of removal. The experiments were approved by the local ethics

committee (protocol number: EA1/180/09). All specimens were chopped to fit into 50 ml Eppendorf tubes. Particular attention was paid when preparing the muscle sample to ensure arrangement of the muscle fibers parallel to the long axis of the tube. Dispersive and nondispersive material behavior was compared using a gel phantom. Therefore, 10 g of WiroGel (Bego, Bremen, Germany) was dissolved in 50 ml of water heated to 90 °C. The solution was filled into a 50 ml Eppendorf tube and stored for two days. During all experiments, temperatures were kept constant from 17 °C to 19 °C. Experiments were repeated three times on different days using different samples of calf brain, bovine liver, and bovine muscle. Only one MRE experiment was run on the gel sample and the fibrotic liver sample.

2.2. Mechanical excitation

A sketch of the experimental setup is shown in Fig. 1. The vibration source was an electromagnetic coil (A) attached to a carbon fiber piston (B) whose position was fixed to the center of the magnet bore (C) by a plastic disk (D) in front of the gradient coil (E). The sample tube (F) was attached to the end of the carbon fiber rod (B) that was inside the MRI coil. All images were acquired in axial orientation (G).

Vibrations were produced by applying a sinusoidal current ranging in frequency between 100 and 800 Hz to an air-cooled Lorentz coil (A) in the fringe field of the MRI scanner (H). Frequency, amplitude, and number of the sinusoidal oscillation cycles were controlled by an arbitrary function generator (I) connected via audio amplifier (J) to the driving coil. Although the vibration coil produced mainly vertical oscillations, significant horizontal vibration components were observed, which most presumably resulted from mode conversions of bending waves of the actuator piston on the vessel walls of the sample tube. The vibration was initiated by a trigger pulse from the control unit (K) of the scanner whose timing was defined by a modified imaging sequence at the host computer (L).

2.3. Data acquisition

All measurements were performed on a 7T scanner (Bruker PharmaScan 70/16, Ettlingen, Germany) running ParaVision 4.0 software and using a 38 mm bore rat head coil. A FLASH sequence (Fig. 2) was customized for MRE by sinusoidal motion sensitizing gradients (MSG) in the through-plane direction. The MSG strength was 285 mT/m with frequencies 100–800 Hz matched to the mechanical vibration. The number of the MSG periods varied with frequency from 1 to 8 in order to keep a constant echo time (TE) of 16 ms. To compensate for static phase contributions, phase difference images were calculated from two images differing in the sign of the MSG. Temporal resolution of the wave propagation was achieved by shifting the trigger in 16 equal time steps over a vibration period resulting in about 20 min total measurement time per MRE experiment. Further

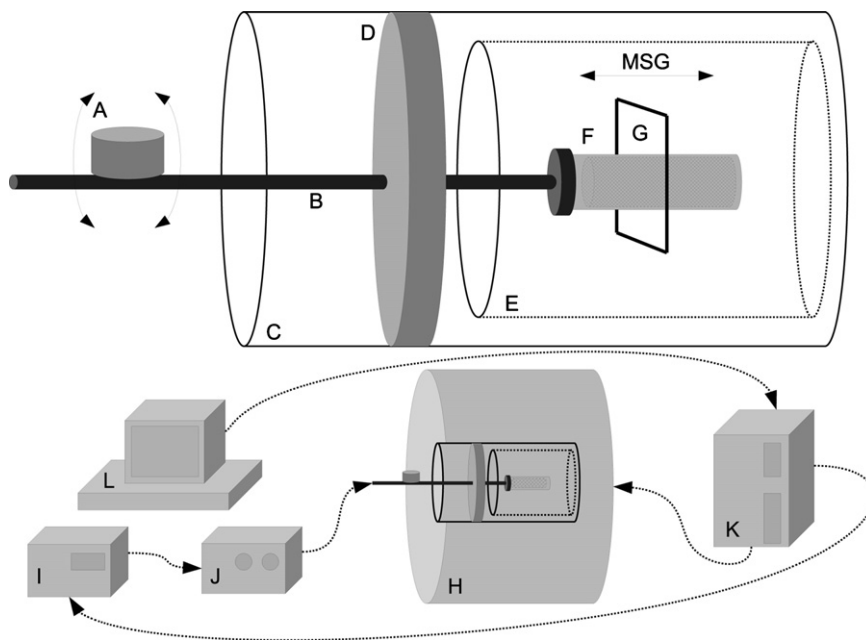


Fig. 1. Setup of vibration coil (A), transducer piston (B), center mount (D), RF coil (E), sample container (F), image slice (G), direction of the motion sensitizing gradient (MSG) relative to the magnet of the MRI scanner (H). The direction of induced vibration in the coil (A) is indicated by arrows. The information pathway is illustrated by dotted arrows running from the operator terminal (L) towards the control unit (K) of the scanner, which controls motion encoding and image acquisition and activates the wave form generator (I), which is connected via audio amplifier (J) to the vibration device.

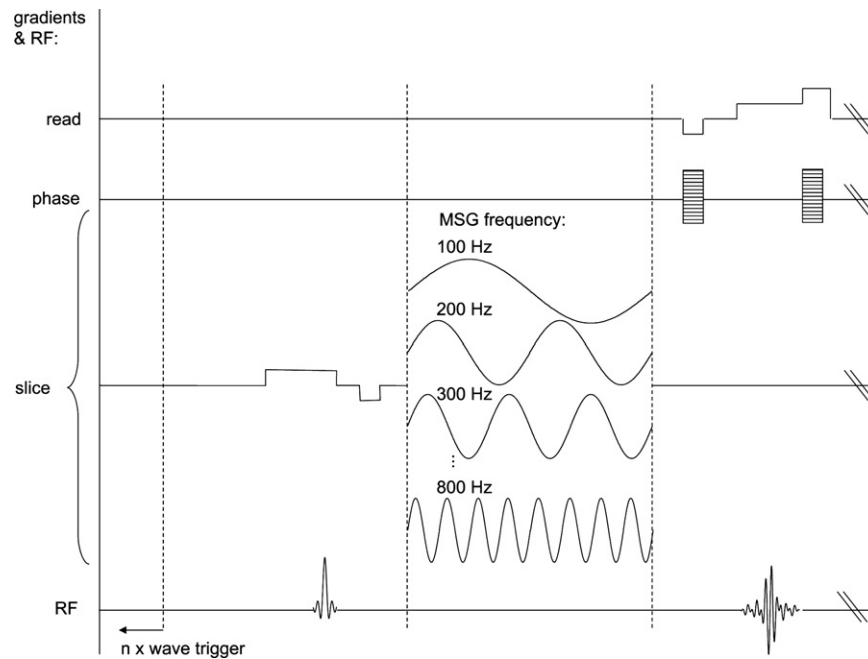


Fig. 2. Modified pulse sequence used for MRE. A standard FLASH sequence was sensitized to motion by a trigger pulse controlling the start of mechanical vibrations relative to the sinusoidal motion sensitizing gradient (MSG). The MSG frequency corresponded to the applied vibration frequency. The wave trigger was shifted 16 times by an increment of a 1/16th of a period of a vibration cycle in order to capture the dynamics of wave propagation.

Table 1
Frequency dependent thresholds for the applied Butterworth bandpass filter.

	Vibration frequency (Hz)							
Threshold (m)	100	200	300	400	500	600	700	800
Upper	0.0035	0.0024	0.0020	0.0018	0.0016	0.0016	0.0015	0.0014
Lower	0.1396	0.0723	0.0474	0.0341	0.0257	0.0199	0.0157	0.0124

acquisition parameters were field of view (FoV)=40 mm, slice thickness=2 mm, 128 × 128 matrix, repetition time (TR)=114–134 ms (depending on tissue sample).

2.4. Data analysis

Image preprocessing comprised subtraction of complex wave images for eliminating static phase shifts, phase unwrapping, and conversion of phases to deflections (in units of microns) by a coefficient incorporating vibration frequency and MSG characteristics (Asbach et al., 2008).

The resulting wave images $u(x,y,t)$, with x and y as spatial coordinates and t as time variable of the propagating shear waves were temporally Fourier-transformed. To remove noise and contributions of compression waves the resulting complex wave images $U(x,y,\omega)$ were filtered using a Butterworth bandpass filter. Empirically derived filter thresholds are summarized in Table 1. A 2D-Helmholtz inversion was applied to the filtered data, yielding the complex shear modulus, $G^*(x,y,\omega)$

$$G^*(x,y,\omega) = -\rho\omega^2 \frac{U(x,y,\omega)}{\Delta U(x,y,\omega)} \quad (1)$$

herein, Δ denotes the 2D-Laplace operator, while ρ is the mass density, which was set to 1000 kg/m³ for all materials. $G^*(x,y,\omega)$ was spatially averaged over a region of interest (ROI) encircling either the entire tissue displayed in the image or a smaller ring containing visually perceptible shear waves. In this way, the ROIs were adapted to the damping of the shear waves since, in liver and brain, CENTRAL parts of the sample were not illuminated by shear waves and had to be excluded from further data processing (Fig. 3). Finally, shear modulus μ and the dimensionless parameter α according to the springpot element were determined by fitting the model function (Klatt et al., 2010a)

$$G_s^*(\omega) = \mu^{1-\alpha} (i\omega\eta)^\alpha \quad (2)$$

to the experimentally observed spatial mean $G^*(\omega)$.

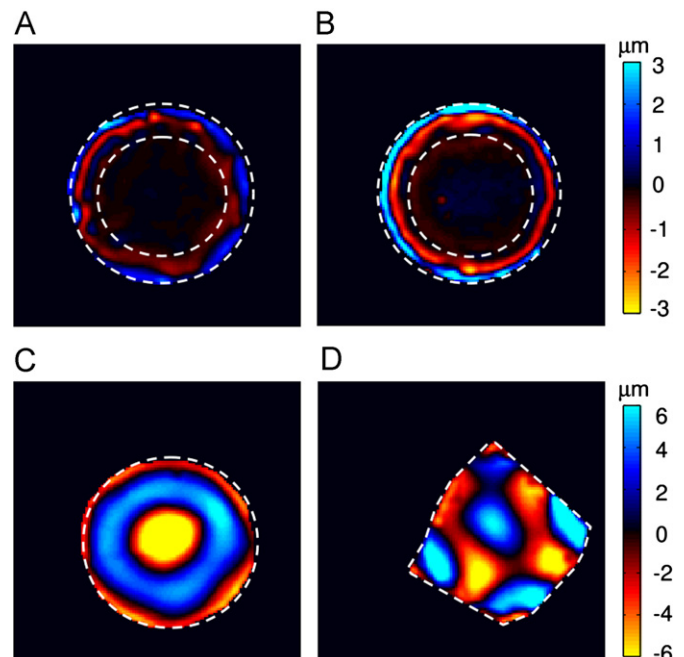


Fig. 3. 600-Hz wave images of calf brain (A), bovine liver (B), bovine muscle (C), and human fibrotic liver (METAVIR score of 3) (D). Dashed white lines demarcate the region of interest (ROI).

3. Results

Fig. 4 shows the real part of complex wave images $U(x,y,\omega)$ of bovine muscle in the frequency range 200–800 Hz. A shortening of the shear wavelengths with increasing excitation frequency is apparent. The wavelengths reflect the elastic properties of the tissues, whereas the viscous properties are revealed by the damping of the mechanical waves. Wavelength and wave damping are represented by storage and loss modulus G' and G'' , respectively, with a solid-like material behavior being characterized by a G''/G' ratio < 1 . In Fig. 5a–d experimental G' and G'' data and corresponding fits based on Eq. (2) are shown for all tissues investigated in this study, all of which display properties of solid materials. In gel, the increase in G' and G'' with ω (Fig. 5a) is comparably small, while all biological tissue samples show a distinctly higher dispersion of the complex modulus (Fig. 5b and d). For liver (Fig. 5b) and brain tissue (Fig. 5d) similar quantities of G'' were observed over the entire frequency range examined. In contrast, muscle tissue has higher values of storage modulus and loss modulus (Fig. 5c). It is important to note that muscle tissue has anisotropic viscoelastic properties (Papazoglou et al., 2005; Deffieux et al., 2009). Our complex modulus values correspond to the viscoelastic properties parallel to muscle fibers, given the aforementioned setup of vibration encoding parallel to fiber alignment (Klatt et al., 2010b). The G'' values parallel to muscle fibers are similar to those measured in our fibrotic liver sample, which are about fifteen times higher than those found in bovine liver. Fig. 6 displays the G''/G' modulus ratios of all samples. A constant ratio indicates the springpot-inherent powerlaw. Although this condition is not fulfilled in all tissues investigated over the entire frequency range, the springpot model seems to be applicable to G'' (400...800 Hz) of bovine liver, to G'' (200...800 Hz) of human fibrotic liver, to G'' (200...600 Hz) of calf brain, and to G'' (300...800 Hz) of bovine muscle. The variation in the modulus ratio of gel is most probably due to reverberations and standing waves, which predominantly occur in nondispersive media. Storage and loss modulus data and their ratios for all biological tissues investigated are summarized in Table 2. Table 3 lists springpot model parameters μ and α of all samples.

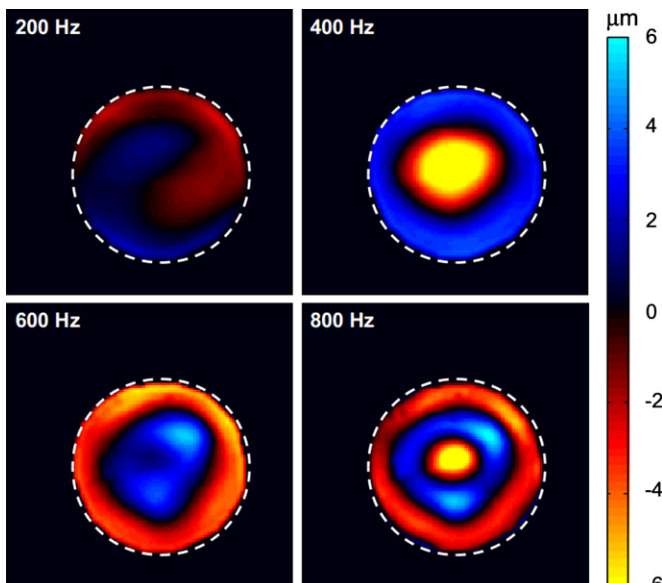


Fig. 4. Wave images of bovine muscle at different vibration frequencies. Dashed white lines demarcate the ROI used for data evaluation.

4. Discussion

This study compares the complex modulus of various biological tissue samples over a wider dynamic range than has been possible by in vivo MRE. The method presented here is, in principle, also applicable to in vivo investigations on small animals such as mice or rats. However, since in vivo systems impose special challenges with regard to geometry and physiological state of the organ under investigation it is of particular importance to first establish a thorough basis of modulus data obtained in excised tissue samples in a defined geometrical shape. The comparability of sample geometry, mechanical stimulus, and data acquisition as achieved in our experimental setup provides insight into the sensitivity of shear waves to tissue structure. For example, we found similar modulus values for liver and brain, which confirms findings of Klatt et al. (2007) using in vivo human MRE with vibration frequencies < 70 Hz and of Bilston et al. (1997), Liu and Bilston (2000), who used oscillatory shear rheometry ≤ 20 Hz. However, due to strong wave absorption, it was not possible to run MRE in brain above 600 Hz, whereas no such enhanced wave attenuation was encountered in liver (with modulus detection up to 800 Hz). Since this difference is obviously not caused by inherent viscoelastic properties we attribute the enhanced wave attenuation in brain to the scattering of shear waves. Shear wave scattering in living brain has been reported by Papazoglou et al. (2009). A further in-depth analysis on phantoms revealed distinct wave absorption up to the limit of localization of shear waves (Papazoglou et al., 2010). Most notably, this does not impact the dispersion of the complex modulus but the penetration depth of the shear waves or their 'mean free path' of propagation. Indeed, our brain sample was much more heterogeneous (due to the presence of sulci and vessels) than liver tissue. Although this certainly changes the transport characteristics of shear waves in biological tissue, the measured complex moduli seem to be uninfluenced by such effects.

Another important aspect of shear-wave-based modulus estimation concerns modulus recovery from wave images by inversion algorithms. Numerous papers have been published on the optimization of time-harmonic wave inversion for elastography (see e.g. (Park and Maniatty, 2006)). Most approaches rely on an algebraic solution of the Helmholtz wave equation for the complex modulus by assuming local homogeneity as given in Eq. (1). With regard to a wider dynamic range of the recovered complex modulus it is important to consider two sources of bias inherent in discrete Helmholtz inversion: (i) the shear wave speed is underestimated in the range of low wave phase gradients (low wave numbers) due to noise and (ii) the shear wave speed is overestimated in the range of high wave phase gradients (short wavelengths) due to the discretization of the waves. Thus an optimum range of pixels per wavelength in the wave image exists. The deviation of the apparent shear wave speed from the true wave speed can be estimated by knowing the SNR of the waves and the number of pixels per wavelengths (Papazoglou et al., 2008). In our experiments on calf brain, the number of pixels displaying a specific wavelength varied from 12 to 77 for vibration frequencies from 600 to 100 Hz. According to Papazoglou et al. (2008) it follows together with our measured SNR of 25 ± 6 that the degree of underestimation of the moduli at 100 Hz should not exceed 7 percent, whereas the maximum degree of overestimation at 600 Hz is about 4.6%. In bovine muscle, the SNR was similar to that achieved in calf brain. However, the wavelengths in muscle were much larger and thus supported by 33 pixels at 800 Hz and by 76 pixels at 200 Hz, yielding a potential underestimation from 2% to 12% over the entire frequency range. Good agreement of MRE-based G'' values

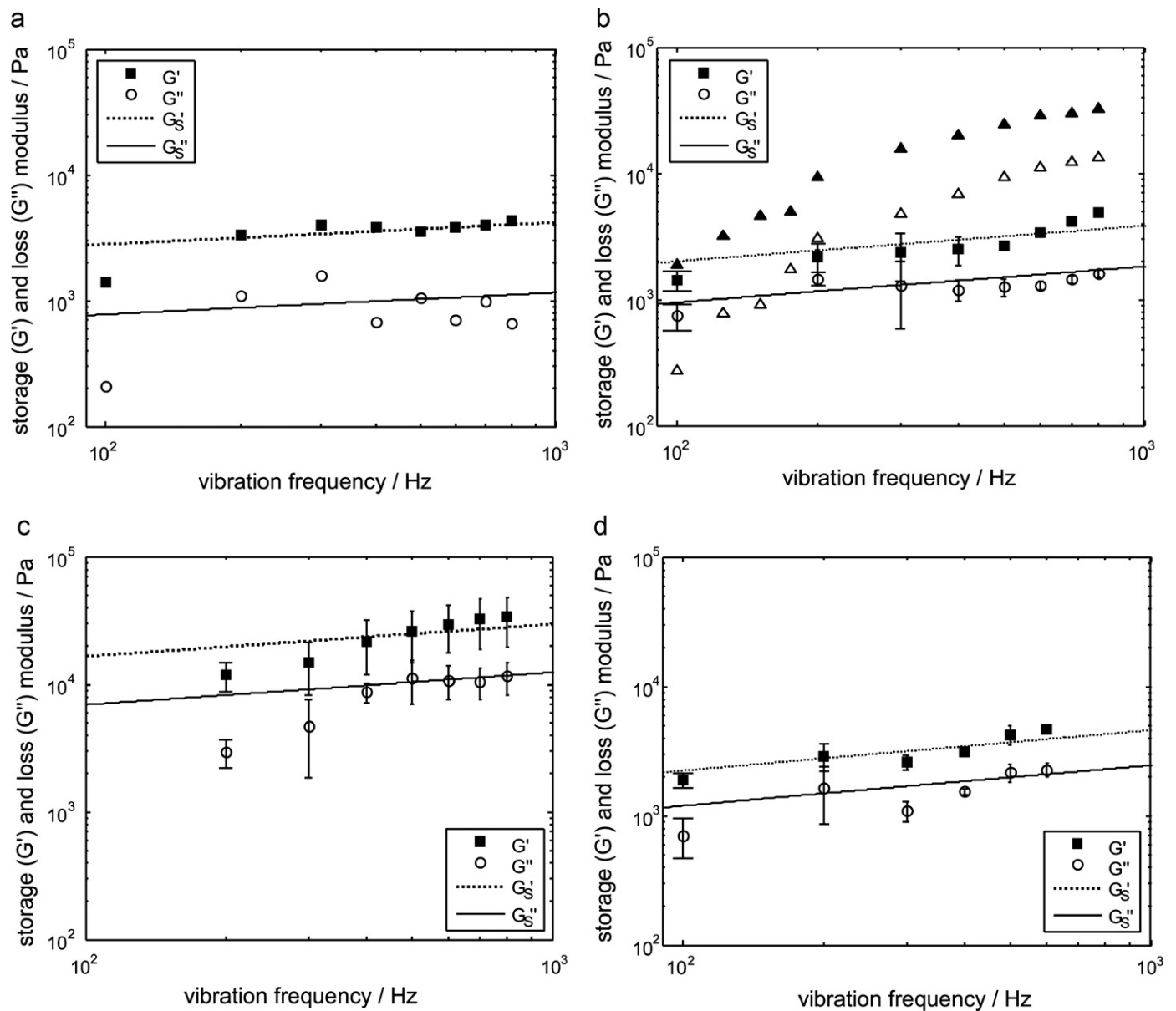


Fig. 5. Experimental data of storage modulus G' (real part of G^* , closed symbols) and loss modulus G'' (imaginary part of G^* , open symbols). Corresponding fits according to the springpot model (Eq. (2)) are shown by dashed lines for G'_S and solid lines for G''_S . Note that the fit lines of G' and G'' are not independent from each other since both slope and relative offset are determined by a single parameter (α). Error bars indicate the standard deviation of three repeated experiments on different days in different samples. (a) Gel phantom; (b) bovine liver, triangles indicate human fibrotic liver; (c) bovine muscle; and (d) calf brain.

of liver measured with different resolution and SNR was demonstrated for a wide dynamic range (Klatt et al., 2010c). Fig. 7 illustrates a combined 1.5T human MRE and 7T micro-MRE study of the same liver specimen. The field of view in the human scanner (192 mm) was almost five times larger than in the animal scanner. Therefore the applicable vibration frequencies were limited to 25–150 Hz but still overlapped with the frequency range of the animal scanner (100–600 Hz). The springpot fit of the combined data resulted in a μ of 7.5 kPa and an α value of 0.32. This agrees well with the structure parameter α deduced from Fig. 5 whereas μ shows a distinct lower value of 3.7 kPa. As the structure of the different liver specimens seems to be conserved, the lower shear elasticity is attributed to different ages and storage conditions of the liver samples.

Comparing the springpot μ we determined with data in the literature requires consideration of the specific sample viscosity underlying this parameter (Klatt et al., 2010a). Unit viscosity

($\eta = 1 \text{ Pa s}$) is implicit in Eq. (2) and thus in all μ -values given in Table 3. Other studies focused on the specific viscous behavior of brain or liver by assuming higher η -values of 3.7 or 7.4 Pa s, respectively, (Sack et al., 2009; Asbach et al., 2010). For comparison, data reported in Table 3 must be transformed by $\mu(\eta) = \eta^{-\alpha/(\alpha-1)} \mu(\eta = 1 \text{ Pa s})$ yielding e.g. $\mu(\eta = 3.7 \text{ Pa s}) = 2.7 \text{ kPa}$ for calf brain, $\mu(\eta = 7.4 \text{ Pa s}) = 1.7 \text{ kPa}$ for bovine liver, and $\mu(\eta = 7.4 \text{ Pa s}) = 20.5 \text{ kPa}$ for human fibrotic liver. These modulus values differ from the values determined by in vivo human MRE, which is most likely attributable to differences in tissue properties within the body and in removed specimens such as temperature effects (a lower sample temperature yields an increasing stiffness (Klatt et al., 2010a)) and effects due to tissue perfusion. Furthermore, even though Fig. 7 presents a good match between low- and high-frequency MRE, differences in the springpot constants will certainly appear by changing the limits of the considered frequency range in the fit.

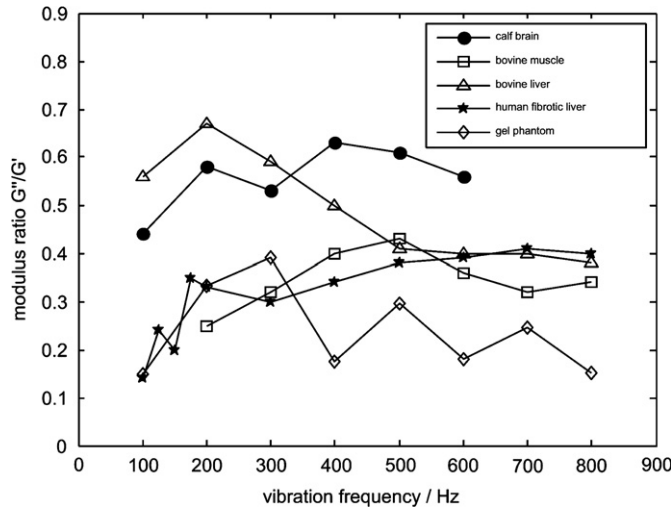


Fig. 6. Experimental G''/G' ratios, which are, by theory, related to the tangent of the dispersion slopes of G'_S and G''_S of the springpot model [$G''_S/G'_S = \tan(\alpha\pi/2)$]. Please note that the variation in gel data is not due to low SNR but attributed to reverberations caused by low wave attenuation in the confined sample.

Table 2

Loss modulus (G''), storage modulus (G'), and G''/G' ratio of calf brain, bovine muscle, bovine liver, and human fibrotic liver. The G''/G' ratios were derived by spatially averaging G'' -maps divided by G' -maps. Error margins correspond to the standard deviation of independent experiments.

Frequency (Hz)	G' (kPa)	G'' (kPa)	G''/G'
<i>(a) Calf brain</i>			
100	1.87 (0.25)	0.71 (0.24)	0.38 (0.09)
200	2.90 (0.66)	1.63 (0.77)	0.56 (0.13)
300	2.60 (0.35)	1.10 (0.19)	0.42 (0.02)
400	3.13 (0.20)	1.54 (0.07)	0.49 (0.02)
500	4.25 (0.70)	2.17 (0.37)	0.51 (0.01)
600	4.64 (0.20)	2.28 (0.28)	0.49 (0.04)
<i>(b) Bovine muscle</i>			
200	11.89 (3.07)	2.93 (0.72)	0.25 (0.06)
300	14.84 (6.62)	4.73 (2.87)	0.32 (0.19)
400	21.92 (10.00)	8.68 (1.48)	0.40 (0.10)
500	26.06 (11.25)	11.16 (4.13)	0.43 (0.03)
600	29.70 (11.95)	10.74 (3.12)	0.36 (0.05)
700	32.87 (13.83)	10.57 (2.96)	0.32 (0.07)
800	34.00 (14.23)	11.55 (3.38)	0.34 (0.07)
<i>(c) Bovine liver</i>			
100	1.42 (0.25)	0.74 (0.18)	0.53 (0.05)
200	2.19 (0.56)	1.46 (0.17)	0.66 (0.12)
300	2.36 (0.95)	1.30 (0.71)	0.55 (0.07)
400	2.50 (0.64)	1.19 (0.23)	0.48 (0.03)
500	2.67 (0.20)	1.26 (0.20)	0.47 (0.04)
600	3.39 (0.19)	1.29 (0.10)	0.38 (0.03)
700	4.14 (0.12)	1.44 (0.11)	0.35 (0.02)
800	4.91 (0.22)	1.62 (0.12)	0.33 (0.01)
<i>(d) Human liver (HCV, METAVIR score 3)</i>			
100	1.90	0.27	0.14
125	3.21	0.78	0.24
150	4.59	0.91	0.20
175	5.01	1.75	0.35
200	9.25	3.06	0.33
300	15.77	4.75	0.30
400	20.20	6.90	0.34
500	24.73	9.41	0.38
600	28.84	11.14	0.39
700	29.99	12.30	0.41
800	32.85	13.28	0.40

In conclusion, a wide-range modulus-dispersion MRE experiment was introduced and applied to various biological tissue samples. Powerlaw simplification of the dispersion function of the

Table 3

Springpot-model constants corresponding to the fit curves shown in Fig. 5.

	Gel	Calf brain	Bovine muscle	Bovine liver	Human liver (fibrotic)
α	0.17	0.31 (0.01)	0.25 (0.02)	0.28 (0.01)	0.34
μ (kPa)	4.0	4.8 (0.3)	56 (23)	3.7 (0.6)	57.5

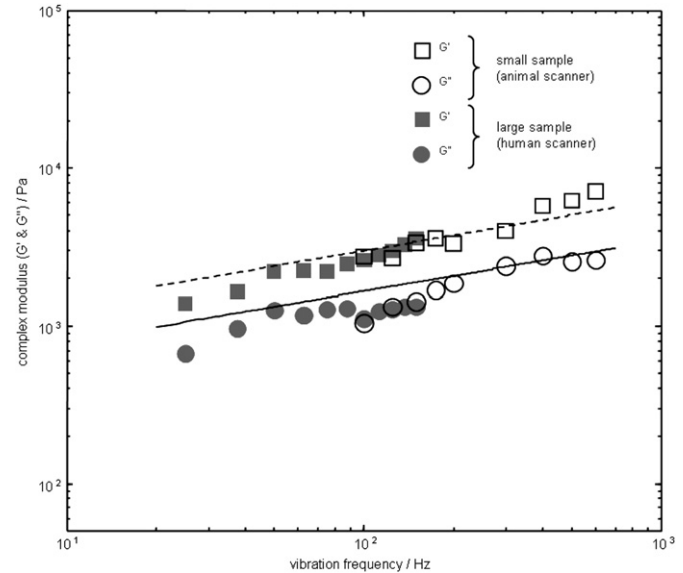


Fig. 7. Combined MRE data of a bovine liver specimen acquired on a 1.5-T human MRI system (solid gray symbols) and a 7-T animal MRI scanner (open symbols). Fit curves according to Eq. (2) (G'_S , dashed line; G''_S solid line) were calculated for $\mu=7.5$ kPa and $\alpha=0.32$.

complex shear modulus yielded two constitutive parameters for each tissue related to elasticity and slope of the modulus dispersion. In this figure, brain and liver tissues present with similar viscoelastic properties, while fibrotic liver displays distinctly higher shear modulus values, similar to the anisotropic elastic constants of excised muscle parallel to the fiber direction. The slope of the modulus dispersion was highest in fibrotic liver, followed by brain, normal liver, and muscle. The lowest dispersion of the complex modulus was seen in a soft gel phantom. These results add important information of the dynamic viscoelastic properties of biological tissues to MRE data acquired in humans and furthermore allow the extension of existing methods to small tissue samples and animal models. In summary, wide-range dynamic MRE combined with a data analysis based on a powerlaw provides an appropriate means for characterizing the mechanical properties of biological soft tissue.

Conflict of interest statement

None of the authors have any conflict of interest.

Acknowledgement

This study was supported by grants of the German Research Foundation Sa 901/3, Sa 901/4, and Br 2235/3-1.

References

- Asbach, P., Klatt, D., Hamhaber, U., Braun, J., Somasundaram, R., Hamm, B., Sack, I., 2008. Assessment of liver viscoelasticity using multifrequency MR elastography. *Magn. Reson. Med.* 60, 373–379.
- Asbach, P., Klatt, D., Schlosser, B., Biermer, M., Muehe, M., Rieger, A., Loddenkemper, C., Somasundaram, R., Berg, T., Hamm, B., Braun, J., Sack, I., 2010. Viscoelasticity-based Staging of Hepatic Fibrosis with Multifrequency MR Elastography. *Radiology*. doi:10.1148/radiol.10092489.
- Atay, S.M., Kroenke, C.D., Sabet, A., Bayly, P.V., 2008. Measurement of the dynamic shear modulus of mouse brain tissue in vivo by magnetic resonance elastography. *J. Biomech. Eng.* 130, 021013.
- Bilston, L.E., Liu, Z., Phan-Thien, N., 1997. Linear viscoelastic properties of bovine brain tissue in shear. *Biorheology* 34, 377–385.
- Deffieux, T., Montaldo, G., Tanter, M., Fink, M., 2009. Shear wave spectroscopy for in vivo quantification of human soft tissues visco-elasticity. *IEEE Trans. Med. Imaging* 28, 313–322.
- Gennisson, J.L., Deffieux, T., Mace, E., Montaldo, G., Fink, M., Tanter, M., 2010. Viscoelastic and anisotropic mechanical properties of in vivo muscle tissue assessed by supersonic shear imaging. *Ultrasound Med. Biol.* 36, 789–801.
- Gurtovenko, A.A., Blumen, A., 2005. *Polymer Analysis, Polymer Theory*. Springer, Berlin, pp. 171–282.
- Hoyt, K., Kneezel, T., Castaneda, B., Parker, K.J., 2008. Quantitative sonoelastography for the in vivo assessment of skeletal muscle viscoelasticity. *Phys. Med. Biol.* 53, 4063–4080.
- Huwart, L., Sempoux, C., Salameh, N., Jamart, J., Annet, L., Sinkus, R., Peeters, F., ter Beek, L.C., Horsmans, Y., Van Beers, B.E., 2007. Liver fibrosis: noninvasive assessment with MR elastography versus aspartate aminotransferase-to-platelet ratio index. *Radiology* 245, 458–466.
- Klatt, D., Friedrich, C., Korth, Y., Vogt, R., Braun, J., Sack, I., 2010a. Viscoelastic properties of liver measured by oscillatory rheometry and multifrequency magnetic resonance elastography. *Biorheology* 47, 133–141.
- Klatt, D., Hamhaber, U., Asbach, P., Braun, J., Sack, I., 2007. Noninvasive assessment of the rheological behavior of human internal organs using multifrequency MR elastography: a study of brain and liver viscoelasticity. *Phys. Med. Biol.* 52, 7281–7294.
- Klatt, D., Papazoglou, S., Braun, J., Sack, I., 2010b. Viscoelasticity-based magnetic resonance elastography of skeletal muscle. *Phys. Med. Biol.* 55, 6445–6459.
- Klatt, D., Stiller, D., Kaulisch, T., Nießen, H., Riek, K., Papazoglou, S., Elgeti, T., Sack, I., Braun, J., 2010c. Wide dynamic range MR elastography of liver. In: *Proceedings of 18th Scientific Meeting, International Society for Magnetic Resonance in Medicine* (Stockholm).
- Liu, Z., Bilston, L., 2000. On the viscoelastic character of liver tissue: experiments and modelling of the linear behaviour. *Biorheology* 37, 191–201.
- Muthupillai, R., Lomas, D.J., Rossman, P.J., Greenleaf, J.F., Manduca, A., Ehman, R.L., 1995. Magnetic resonance elastography by direct visualization of propagating acoustic strain waves. *Science* 269, 1854–1857.
- Ophir, J., Cespedes, I., Ponnekanti, H., Yazdi, Y., Li, X., 1991. Elastography: a quantitative method for imaging the elasticity of biological tissues. *Ultrason. Imaging* 13, 111–134.
- Othman, S.F., Xu, H., Royston, T.J., Magin, R.L., 2005. Microscopic magnetic resonance elastography (microMRE). *Magn. Reson. Med.* 54, 605–615.
- Papazoglou, S., Braun, J., Hamhaber, U., Sack, I., 2005. Two-dimensional waveform analysis in MR elastography of skeletal muscles. *Phys. Med. Biol.* 50, 1313–1325.
- Papazoglou, S., Hamhaber, U., Braun, J., Sack, I., 2008. Algebraic Helmholtz inversion in planar magnetic resonance elastography. *Phys. Med. Biol.* 53, 3147–3158.
- Papazoglou, S., Klatt, D., Braun, J., Sack, I., 2010. Anderson localization of shear waves observed by magnetic resonance imaging. *Eur. Phys. Lett.* 91, 17007.
- Papazoglou, S., Xu, C., Hamhaber, U., Siebert, E., Bohner, G., Klingebiel, R., Braun, J., Sack, I., 2009. Scatter-based magnetic resonance elastography. *Phys. Med. Biol.* 54, 2229–2241.
- Park, E., Maniatty, A.M., 2006. Shear modulus reconstruction in dynamic elastography: time harmonic case. *Phys. Med. Biol.* 51, 3697–3721.
- Sack, I., Beierbach, B., Wuerfel, J., Klatt, D., Hamhaber, U., Papazoglou, S., Martus, P., Braun, J., 2009. The impact of aging and gender on brain viscoelasticity. *Neuroimage* 46, 652–657.
- Salameh, N., Larrat, B., Abarca-Quinones, J., Pallu, S., Dorvillius, M., Leclercq, I., Fink, M., Sinkus, R., Van Beers, B.E., 2009. Early detection of steatohepatitis in fatty rat liver by using MR elastography. *Radiology* 253, 90–97.
- Schiessel, H., Blumen, A., 1995. Mesoscopic pictures of the sol–gel transition—ladder models and fractal networks. *Macromolecules* 28, 4013–4019.
- Sinkus, R., Siegmund, K., Xydeas, T., Tanter, M., Claussen, C., Fink, M., 2007. MR elastography of breast lesions: understanding the solid/liquid duality can improve the specificity of contrast-enhanced MR mammography. *Magn. Reson. Med.* 58, 1135–1144.
- Vappou, J., Breton, E., Choquet, P., Goetz, C., Willinger, R., Constantinesco, A., 2007. Magnetic resonance elastography compared with rotational rheometry for in vitro brain tissue viscoelasticity measurement. *J. Magn. Mater.* 20, 273–278.
- Wuerfel, J., Paul, F., Beierbach, B., Hamhaber, U., Klatt, D., Papazoglou, S., Zipp, F., Martus, P., Braun, J., Sack, I., 2010. MR-elastography reveals degradation of tissue integrity in multiple sclerosis. *Neuroimage* 49, 2520–2525.
- Yin, M., Talwalkar, J.A., Glaser, K.J., Manduca, A., Grimm, R.C., Rossman, P.J., Fidler, J.L., Ehman, R.L., 2007. Assessment of hepatic fibrosis with magnetic resonance elastography. *Clin. Gastroenterol. Hepatol.* 5, 1207–13 e2.
- Ziol, M., Handra-Luca, A., Kettaneh, A., Christidis, C., Mal, F., Kazemi, F., de Ledinghen, V., Marcellin, P., Dhumeaux, D., Trinchet, J.C., Beaugrand, M., 2005. Noninvasive assessment of liver fibrosis by measurement of stiffness in patients with chronic hepatitis C. *Hepatology* 41, 48–54.